Published in final edited form as:
J Magn Reson Imaging. 2008 March ; 27(3): 659–665. doi:10.1002/jmri.21278.

Fast Four-Dimensional Coronary MR Angiography With k-t GRAPPA

Peng Lai, MS[1,2], **Feng Huang, PhD**[3], **Andrew C. Larson, PhD**[2], and **Debiao Li, PhD**[1,2,*]

[1] Department of Biomedical Engineering, Northwestern University, Chicago, Illinois

[2] Department of Radiology, Northwestern University, Chicago, Illinois

[3] Advanced Concept Development, Invivo Corporation, Gainesville, Florida

Abstract

Purpose—To investigate the effectiveness of k-t GRAPPA for accelerating four-dimensional (4D) coronary MRA in comparison with GRAPPA and the feasibility of combining variable density undersampling with conventional k-t GRAPPA (k-t^2 GRAPPA) to alleviate the overhead of acquiring autocalibration signals.

Materials and Methods—The right coronary artery of nine healthy volunteers was scanned at 1.5 Tesla. The 4D *k*-space datasets were fully acquired and subsequently undersampled to simulate partially parallel acquisitions, namely, GRAPPA, k-t GRAPPA, and k-t^2 GRAPPA. Comparisons were made between the images reconstructed from full k-space datasets and those reconstructed from undersampled k-space datasets.

Results—k-t GRAPPA significantly reduced artifacts compared with GRAPPA and high acceleration factors were achieved with only minimal sacrifices in vessel depiction. k-t^2 GRAPPA could further increase imaging speed without significant losses in image quality.

Conclusion—By exploiting high-degree spatiotemporal correlations during the rest period of a cardiac cycle, k-t GRAPPA and k-t^2 GRAPPA can greatly increase data acquisition efficiency and, therefore, are promising solutions for fast 4D coronary MRA.

Keywords

4D coronary MRA; fast imaging; k-t GRAPPA

Despite advances in MR technology, high-quality coronary MR angiography (MRA) remains challenging and its clinical value remains limited. A major difficulty has been in the achievable scan time restricted by cardiac and respiratory motion of the heart as well as various technical (e.g., gradient amplitude) and physiological (e.g., nerve stimulation) constraints. Furthermore, suppression of cardiac motion continues to be a critical concern in coronary MRA. For conventional electrocardiogram citation(ECG) triggered segmented data acquisition (1,2), because the pattern of cardiac motion can vary markedly between different subjects and even different coronary artery segments in the same subject (3,4), accurate determination of the optimal trigger delay times remains a significant complication. Recently, four-dimensional (4D) coronary MRA was proposed to better resolve cardiac motion (5). By reconstructing contiguous cardiac frames, cardiac motion throughout the entire cardiac cycle can be assessed and the cardiac phases with superior coronary artery depiction can be retrospectively selected. However, this time-resolved strategy inherently requires sufficiently high temporal resolution

*Address reprint requests to: D.L., Suite 700, 448 East Ontario Street, Chicago, IL 60611. d-li2@northwestern.edu.

to suppress cardiac motion and, therefore, poses even more rigorous demands on data acquisition efficiency.

Over the past years, several fast imaging techniques have been proposed for cardiovascular MRI applications. A vast majority of these techniques attempt to undersample *k*-space without compromising image quality (6–13). Sensitivity encoding (SENSE) (8) and generalized autocalibrating partially parallel acquisitions (GRAPPA) (9) take advantage of spatially varying coil sensitivity to unfold alias artifacts within the image domain or derive unsampled *k*-space data. Alternatively, it has been shown that correlations along the temporal dimension can be used to accelerate data acquisition. In these temporal correlation-based methods, *k*-space data are collected in full over successive time points but only partially acquired at each time point. The *k*-space undersampling was resolved by either estimating the missing data from data at neighboring time points (5–7) or eliminating the alias artifacts from the outer portion of the field of view (FOV) by temporal filtering (10). Also, another category of spatiotemporal approaches, namely, adaptive sensitivity encoding incorporating temporal filtering (TSENSE) (11), k-t BLAST/SENSE (12), and k-t GRAPPA (13), exploit correlations in both *k*-space and time to reduce residual artifacts and achieve higher acquisition efficiency.

As cardiac motion is quasiperiodic, coronary artery images at adjacent cardiac phases exhibit a high degree of correlations. This property suggests that the spatiotemporal strategies may offer promising solutions for the aforementioned stringent requirements for 4D coronary MRA. In this work, the effectiveness of k-t GRAPPA in 4D coronary MRA was investigated. However, conventional k-t GRAPPA requires sequential sampling of several center *k*-space lines as autocalibration signals (ACS) at each time point. Such complete sampling of ACS lines significantly impacts acquisition efficiency (14), particularly for high acceleration factors. Although the number of ACS lines could be reduced to compensate for this effect, the image quality would be sacrificed. To address this problem, a modified k-t GRAPPA method capable of exploiting spatiotemporal correlations in both ACS lines and outer *k*-space lines was proposed. Full 4D *k*-space data were acquired in volunteer experiments and partially parallel acquisitions for fast imaging were simulated by decimating the full *k*-space data offline. Statistical analyses based on artifact level and vessel delineation were performed to evaluate the efficacy of each of these fast imaging approaches.

MATERIALS AND METHODS

Modified k-t GRAPPA

In conventional k-t GRAPPA, the ACS lines are acquired at center *k*-space. The low-frequency information contained in the ACS lines changes relatively slower than high-frequency information along the time dimension. Therefore, acquisition of the ACS lines with moderate undersampling in k-t space should retain sufficient information for accurate coil sensitivity estimation and image reconstruction, especially at mid-diastole when cardiac motion is minimal. Based on this hypothesis, spatiotemporal correlations in these center *k*-space lines were exploited by combining k-t GRAPPA with variable density undersampling to reduce the overhead of ACS acquisition. In the modified approach, the outer *k*-space lines and the ACS lines were undersampled by two independent acceleration factors. The undersampling was performed in a time-interleaved manner in both *k*-space regions so as to more completely exploit spatiotemporal correlations. Accordingly, the image reconstruction consisted of two steps. First, k-t GRAPPA without ACS was performed to recover the missing ACS lines at all cardiac phases (13). Next, weighting coefficients were estimated from the ACS lines and the unsampled outer *k*-space lines were recovered using conventional k-t GRAPPA with ACS. This modified approach performing k-t GRAPPA in the ACS lines and the entire *k*-space successively is termed k-t^2 GRAPPA. For simplicity, acceleration factors in outer *k*-space

(AFO) and center *k*-space (AFC) will be used to depict the sampling pattern for the partially parallel acquisitions described in this work.

Selection of a higher AFC enables faster data acquisition but potentially introduces severe temporal blurring. For this work, the optimal AFC for k-t^2 GRAPPA was determined based on volunteer studies. Data acquisition for k-t^2 GRAPPA was simulated with an AFO of 5 and AFCs of 1~6, as will be described later. The relative errors in the reconstructed mid-diastole images with different AFCs were calculated. The AFC providing a desirable compromise between imaging speed and the reconstruction error was selected as the optimal AFC and used for k-t^2 GRAPPA with all AFO values. However, general determination of the optimal AFC goes beyond the current scope of this work.

Acquisition of Full k-Space Data

Human studies were conducted in nine healthy volunteers (mean heart rate: 66 ± 9 beats/min) using a 1.5 Tesla Magnetom Sonata clinical MRI scanner (Siemens Medical Solutions, Erlangen, Germany) and an eight-channel phased-array cardiac coil (four anterior and four posterior channels). Written consent was obtained from each volunteer before each study with the approval of our institutional review board. In each volunteer, the right coronary artery was localized and 4D coronary MRA was performed. Raw *k*-space datasets were collected using a respiratory self-gating (RSG) SSFP sequence with Cartesian sampling (15). Data acquisition was similar to that of a conventional segmented cine sequence with retrospective cardiac gating, but an additional *k*-space center line (RSG line) was acquired before each segmented data acquisition to track breathing-induced heart motion. Furthermore, the same data acquisition per cardiac phase of a heartbeat was repeated for 4 s to approximately cover one respiratory cycle.

Imaging parameters for these studies included 320–350 × 220–250 mm^2 FOV (depending on the size of the volunteer), 8 partitions interpolated from 4, 1.75 mm slice thickness after interpolation, 256 × 165 matrix size, 1.25–1.37 × 1.33–1.51 mm^2 in-plane resolution, 60° flip angle, TE!TR $ 2.15!4.3 ms, 11 lines for each cardiac phase/heartbeat. The scan time was 4 min for each volunteer.

The raw *k*-space data were collected continuously with free-breathing and retrospectively processed to resolve cardiac and respiratory motion. First, the raw data were rebinned into 15 evenly spaced cardiac phases based on the simultaneously recorded ECG signal (16). Next, the breathing-induced heart motion during the scan was derived from the RSG lines, and the full 4D *k*-space for image reconstruction was subsequently calculated by applying retrospective respiratory gating and motion compensation as described previously (15).

Simulation of Partial Parallel Acquisitions

The *k*-space datasets for k-t GRAPPA and k-t^2 GRAPPA with one-dimensional acceleration were extracted from the full 4D *k*-space offline. For k-t GRAPPA, the outer *k*-space lines were decimated in the phase-encoding direction by an AFO in a time-interleaved manner, while the ACS lines at center *k*-space were sequentially sampled. As an example, Figure 1 illustrates the sampling pattern for k-t GRAPPA with an AFO of 4. *k*-space sampling in the outer *k*-space was skewed in the temporal direction and different sets of phase-encoding lines were extracted at four successive time points. At each cardiac phase, *k*-space lines were decimated by skipping every three phase-encoding lines, but a few ACS lines located at center *k*-space were sampled with full-FOV phase-encoding spacing. For k-t^2 GRAPPA, data acquisition was simulated with high AFOs. The difference from k-t GRAPPA is that time-interleaved undersampling was also performed in ACS lines. As the example shown in Figure 1, ACS acquisition is skewed in the temporal direction with an AFC of 3.

Because GRAPPA is a widely adopted technique for fast imaging, data acquisition for GRAPPA was also simulated by decimating the same full *k*-space data-sets. Different from the time-interleaved sampling patterns described above, the same set of phase-encoding lines were repeatedly sampled at all cardiac phases. Table 1 shows the sampling parameters for GRAPPA, k-t GRAPPA, and k-t^2 GRAPPA and the corresponding net reduction factors, defined as the ratio of the number of the total sampled *k*-space lines to the number of the *k*-space lines required for full-FOV reconstruction. To balance the increasing effect of ACS acquisition on the net reduction factor, smaller ACS line numbers were used for higher acceleration factors.

Image Reconstruction and Image Quality Analysis

The 4D cardiac frames were reconstructed offline from the sparsely sampled GRAPPA, k-t GRAPPA, and k-t^2 GRAPPA *k*-space datasets as well as the full *k*-space datasets. For GRAPPA implementation, the size of convolution kernel was 4 (phase-encoding direction) × 5 (frequency-encoding direction). For the implementation of k-t GRAPPA, the description in the original paper (13) was followed. k-t^2 GRAPPA image reconstruction was performed according to the two steps described above. Next, a phase-sensitive method was used to suppress fat signal (17,18) in all the reconstructed images. All offline processing was implemented in the MATLAB environment (MathWorks Inc., Natick, MA).

Image quality with regard to artifact level and vessel delineation was evaluated to investigate the performance of k-t GRAPPA and k-t^2 GRAPPA in comparison with GRAPPA. Unlike cardiac cine imaging, in 4D coronary MRA, the frames with the best vessel delineation, presumably at mid-diastole, are distinctively of superior diagnostic value. Therefore, only mid-diastole identified individually in each subject by retrospectively selecting the cardiac phase providing the best vessel delineation was considered in the following image quality evaluation.

Residual Artifacts

To quantitatively assess the residual artifact level in the images reconstructed using fast imaging techniques, the full *k*-space images were used as the references and artifact power (AP) defined as the normalized power of the artifact image was calculated according to Eq. [1].

$$AP = \frac{\sum_j \| I_j^{ref} |^2 - |I'_j|^2 |}{\sum_j |I_j^{ref}|^2} \quad (1)$$

where I' is the image for evaluation, I_{ref} is the reference image, and j is the index of the image pixel.

Vessel Delineation

The mid-diastole maximum-intensity-projection (MIP) images from the nine volunteers were displayed on nine separate slides. For each slide, the placement of the reference image and the GRAPPA, k-t GRAPPA, and k-t^2 GRAPPA images was randomized. The images were independently scored by two experienced cardiac MRI specialists blinded to the reconstruction techniques. A scoring system (0–4) was used to assess the image quality based on coronary artery visualization: score 0, completely uninterpretable (coronary artery invisible); score 1, poor (coronary artery visible, with markedly blurred borders or markedly delusive artifacts); score 2, acceptable (coronary artery visible, with moderately blurred borders or moderately delusive artifacts); score 3, good (coronary artery visible, with mildly blurred borders or mildly

delusive artifacts); score 4, excellent (coronary visible, with sharply defined borders and no delusive artifacts).

To study the impact of increasing the acceleration factor, the AP values and mean scores of the images with different AFOs were compared with those of the reference images. Additionally, comparison was also performed between (i) GRAPPA and k-t GRAPPA images, (ii) k-t GRAPPA and k-t^2 GRAPPA images, with the same AFOs so as to investigate the effectiveness of different fast-imaging techniques. For the above analyses we used the Wilcoxon signed rank test with a significance level of 0.05.

True k-t Sampling

To validate the performance of k-t^2 GRAPPA with clinical relevant spatial resolution, single-breath-hold 4D coronary MRA was performed on two volunteers using true k-t data acquisition. The following parameters were used: 320 × 250 mm^2 FOV, 320 × 228 matrix, 1.0 × 1.1 mm^2 in-plane resolution, 12 partitions interpolated from 6, 1.5 mm slice thickness after interpolation, 12 lines for each cardiac phase/heartbeat, 60° flip angle, 15 ACS lines, AFO of 5, and AFC of 3. The corresponding net reduction factor was 4.75. Both scans were completed in 24 heartbeats during one breath-hold.

RESULTS

Figure 2 demonstrates the relationship between the mean relative error and the net reduction factor with AFCs of 1~6. Clearly, the relative error increases as the AFC increases. With an AFC up to 3, selection of a larger AFC does not result in a remarkable increase in reconstruction error but improves imaging speed substantially. However, further increasing the AFC above 3 introduces remarkably larger errors with little additional benefit in imaging speed. Therefore, an AFC of 3 was selected for all remaining k-t^2 GRAPPA reconstructions described in this work.

Figure 3a,b,d show the reference MIP images at the even-numbered cardiac phases and the corresponding k-t GRAPPA images with an AFO of 4 and k-t^2 GRAPPA images with an AFO of 4 and AFC of 3. In all these image sets, cardiac motion throughout the entire cardiac cycle in the imaging volume is captured and the cardiac frame best visualizing the coronary artery can be retrospectively selected. In this subject, the best vessel delineation is achieved at mid-diastole (cardiac phase 12). By comparing different image sets at the same cardiac phases, we can see that both k-t GRAPPA and k-t^2 GRAPPA images provide very similar image quality with the reference image at cardiac phase 12. However, distinguishable artifacts and blurring appeared at other cardiac phases, particularly for fine structures, such as the papillary muscles at cardiac phase 2 and the coronary artery at cardiac phase 8. These features are better displayed in the absolute error plots in Figure 3c,e. For both k-t GRAPPA and k-t^2 GRAPPA, the error level clearly exhibits a cardiac phase dependent pattern and is the lowest at mid-diastole. Compared with k-t GRAPPA, k-t^2 GRAPPA produced similar reconstruction errors at mid-diastole, but much larger errors at other cardiac phases.

Figure 4 shows the reference image at mid-diastole from another subject and the corresponding GRAPPA, k-t GRAPPA, and k-t^2 GRAPPA images with various AFOs. Very similar image quality can be observed in the reference image and the k-t GRAPPA and k-t^2 GRAPPA images with AFOs up to 4. When the AFO is increased to 5, although some signal drop appears in the middle of the coronary artery segment, vessel depiction is still not substantially compromised. Contrarily, using GRAPPA, the image is contaminated by distinguishably increased noise and artifacts and the coronary artery becomes almost uninterpretable with an AFO of 4.

Figure 5 illustrates the measured AP values in the GRAPPA, k-t GRAPPA, and k-t^2 GRAPPA images. For all three techniques, the artifact level increases quasilin-early as the acceleration factor increases. However, the fitted slope for k-t GRAPPA (0.034) and k-t^2 GRAPPA (0.021) are much smaller than that for GRAPPA (0.168). Furthermore, the difference between the APs for GRAPPA and those for k-t GRAPPA with the same AFO's is statistically significant ($P < 0.05$), while the difference between k-t GRAPPA and k-t^2 GRAPPA APs is not significant ($P > 0.05$).

The mean scores of vessel delineation are shown in Figure 6. Similar to AP, vessel delineation degrades with a larger AFO. Compared with the reference images, the GRAPPA images with an AFO of 3 and 4 were scored significantly lower ($P < 0.05$) by both reviewers. To reviewer 1, even GRAPPA with an AFO of 2 degrades vessel delineation significantly ($P < 0.05$). On the contrary, using k-t GRAPPA, vessel delineation is not significantly affected with an acceleration factor up to 4 ($P > 0.05$). Furthermore, the mean scores for k-t GRAPPA are always significantly higher than those for GRAPPA with the same AFO's ($P < 0.05$). Comparing k-t^2 GRAPPA to k-t GRAPPA, the former obtains scores without significant difference from the latter with the same AFO's ($P > 0.05$). However, according to Table 1, k-t^2 GRAPPA increases the net reduction factor by 20.31%, 17.16%, and 20.09% for AFOs of 4, 5, and 6, respectively. Additionally, with regard to the reference images, no significant difference is observed in the k-t^2 GRAPPA images with an AFO up to 4 ($P > 0.05$). Even with an AFO of 5, the k-t^2 GRAPPA images still maintain at the good-plus quality level (reviewer 1: 3.28 ± 0.19; reviewer 2: 3.14 ± 0.23) and receive scores not significantly lower than the GRAPPA images with an AFO of 2 ($P > 0.05$).

In the images obtained with true k-t^2 GRAPPA data acquisition, no apparent artifacts were observed and good vessel delineation was obtained at mid-diastole. Figure 7 shows the diastolic images obtained from one subject. Coronary artery motion from early-diastole (Fig. 7a) to late-diastole (Fig. 7d) is captured, and the best coronary artery visualization is achieved at mid-diastole (Fig. 7c).

DISCUSSION

In this work, we evaluated the effectiveness of k-t GRAPPA in 4D coronary MRA and proposed a modified approach, k-t^2 GRAPPA, to further improve imaging speed. In our volunteer studies, we observed that the performance of k-t and k-t^2 GRAPPA was not uniform at different cardiac phases. This feature is determined by the nature of these two techniques, which in theory are an extension of GRAPPA in the temporal dimension. Intrinsically, the accuracy with which missing *k*-space data can be recovered is highly dependent on the degree of temporal correlations at adjacent cardiac phases. Because cardiac motion varies remarkably in intensity over a cardiac cycle and reaches a relatively resting period at mid-diastole, the degree of temporal correlations is the highest between diastolic frames and thereby the best image quality is usually achieved at mid-diastole. In this sense, these two k-t approaches are especially beneficial to 4D coronary MRA, in which the best vessel delineation at mid-diastole, instead of characterization of cardiac motion, is the distinctive clinically relevant goal.

Compared with the alternative spatiotemporal techniques, k-t GRAPPA and k-t^2 GRAPPA possess a few desirable features. First, each inherits the advantages of GRAPPA: no requirement for sensitivity map prescans and no FOV limitations (19). Second, k-t GRAPPA and k-t^2 GRAPPA are simple to implement due to the relatively straightforward extension from *k*-space to k-t space. In comparison, k-t BLAST/SENSE requires additional acquisition of training data and covariance estimation. Third, unlike k-t BLAST/SENSE, k-t GRAPPA does not produce elevated errors at beginning and ending time points in dynamic imaging (13). This property, also observed in our studies, is beneficial for 4D coronary MRA, because only limited

number of cardiac frames can be acquired and the mid-diastolic phase is usually close to the end of a cardiac cycle. Nonetheless, these alternative methods are also very promising candidates for 4D coronary MRA. Further studies are needed to compare the effectiveness of these spatiotemporal approaches.

The need for ACS acquisition for GRAPPA-based techniques can dramatically impede increases in imaging speed. For instance, for k-t GRAPPA with an AFO of 5 as described in this work, the actual net reduction factor was only 4.02, although the ACS line number was reduced to 9. TGRAPPA was proposed to eliminate ACS acquisition with full temporal resolution (14). However, TGRAPPA does not take advantage of temporal correlations and, therefore, generates much larger noise than k-t GRAPPA (13). Alternatively, k-t GRAPPA without ACS also enables full acceleration of the data acquisition. However, this approach uses a uniform under-sampling pattern in the entire *k*-space. When a high acceleration factor is used, significantly enhanced artifacts can be generated compared with k-t GRAPPA with ACS due to large errors at center *k*-space (13). In comparison, k-t^2 GRAPPA offers a flexible method to exploit spatiotemporal correlations in different *k*-space regions. Undersampling of ACS lines and outer *k*-space is performed independently, such that proper AFC and AFO can be determined individually to achieve an optimal compromise between acquisition efficiency and image quality. Additionally, k-t GRAPPA without ACS was implemented in k-t^2 GRAPPA to recover the missing ACS lines. Therefore, compared with using a sliding window like TGRAPPA, temporal fidelity can be better preserved and less temporal blurring is introduced (13).

A few limitations of our current work are also worth noting. First, full 4D *k*-space was acquired during free-breathing to reconstruct the reference images, requiring extremely large raw data size. Therefore, due to the memory limit of the scanner, the achievable spatial resolution was relatively low in the simulation studies. However, this finding should not be a limitation for the eventual application of this technique, as demonstrated by the preliminary results with higher spatial resolution obtained from 2 volunteers. Second, the phase sensitive method used to resolve fat saturation in this work is susceptible to partial volume effects, which can lead to reduced lumen size of the coronary arteries (17,18). In future implementation of 4D coronary MRA, spectrally selective suppression with SSFP (20), a new fat suppression technique that can potential overcome this partial volume problem, should be used. Furthermore, the performance of k-t/k-t^2 GRAPPA for 4D coronary MRA intrinsically depends on the mid-diastolic duration of the subject. The evaluation in this work was based on studies performed on healthy volunteers. Because patients may have higher heart rates and thus shorter diastolic windows, further studies on patients are needed to validate the effectiveness of k-t/k-t^2 GRAPPA in the clinical setting.

In conclusion, this study has demonstrated that k-t GRAPPA and k-t^2 GRAPPA are efficient solutions for high-quality fast 4D coronary MRA. In comparison with conventional GRAPPA, each provides superior image quality in terms of both artifact level and vessel delineation. k-t^2 GRAPPA can greatly reduce the overhead of ACS acquisition without significantly sacrificing coronary artery depiction such that high acquisition efficiency can be achieved enabling high spatial-resolution 4D coronary MRA within a single breath-hold.

Acknowledgments

Contract grant sponsor: National Institute of Health; Contract grant numbers: NIBIB EB002623, NHLBI HL079148; Contract grant sponsor: Siemens Medical Solutions USA, Inc., Malvern, PA.

References

1. Manning WJ, Li W, Boyle NG, Edelman RR. Fat-suppressed breath-hold magnetic resonance coronary angiography. Circulation 1993;87:94–104. [PubMed: 8419029]
2. Duerinckx A, Atkinson DP. Coronary MR angiography during peak-systole: work in progress. J Magn Reson Imaging 1997;7:979–986. [PubMed: 9400840]
3. Wang Y, Vidan E, Bergman GW. Cardiac motion of coronary arteries: variability in the rest period and implications for coronary MR angiography. Radiology 1999;213:751–758. [PubMed: 10580949]
4. Johnson KR, Patel SJ, Whigham A, Hakim A, Pettigrew RI, Oshinski JN. Three-dimensional, time-resolved motion of the coronary arteries. J Cardiovasc Magn Reson 2004;6:663–673. [PubMed: 15347131]
5. Bi X, Park J, Larson AC, Zhang Q, Simonetti O, Li D. Contrast-enhanced 4D radial coronary artery imaging at 3.0 T within a single breath-hold. Magn Reson Med 2005;54:470–475. [PubMed: 16032681]
6. Doyle M, Walsh EG, Blackwell GG, Pohost GM. Block regional interpolation scheme for k-space (BRISK): a rapid cardiac imaging technique. Magn Reson Med 1995;33:163–170. [PubMed: 7707905]
7. Parrish T, Hu X. Continuous update with random encoding (CURE): a new strategy for dynamic imaging. Magn Reson Med 1995;33:326–336. [PubMed: 7760701]
8. Pruessmann KP, Weiger M, Scheidegger MB, Boesiger P. SENSE: sensitivity encoding for fast MRI. Magn Reson Med 1999;42:952–962. [PubMed: 10542355]
9. Griswold MA, Jakob PM, Heidemann RM, et al. Generalized autocalibrating partially parallel acquisitions (GRAPPA). Magn Reson Med 2002;47:1202–1210. [PubMed: 12111967]
10. Madore B, Glover GH, Pelc NJ. Unaliasing by fourier-encoding the overlaps using the temporal dimension (UNFOLD), applied to cardiac imaging and fMRI. Magn Reson Med 1999;42:813–828. [PubMed: 10542340]
11. Kellman P, Epstein FH, McVeigh ER. Adaptive sensitivity encoding incorporating temporal filtering (TSENSE). Magn Reson Med 2001;45:846–852. [PubMed: 11323811]
12. Tsao J, Boesiger P, Pruessmann KP. k-t BLAST and k-t SENSE: dynamic MRI with high frame rate exploiting spatiotemporal correlations. Magn Reson Med 2003;50:1031–1042. [PubMed: 14587014]
13. Huang F, Akao J, Vijayakumar S, Duensing GR, Limkeman M. k-t GRAPPA: a k-space implementation for dynamic MRI with high reduction factor. Magn Reson Med 2005;54:1172–1184. [PubMed: 16193468]
14. Breuer FA, Kellman P, Griswold MA, Jakob PM. Dynamic autocalibrated parallel imaging using temporal GRAPPA (TGRAPPA). Magn Reson Med 2005;53:981–985. [PubMed: 15799044]
15. Lai, PLA.; Park, J.; Carr, JC.; Li, D. Respiratory self-gated 4D coronary MRA. Proceedings of the 14th Annual Meeting of ISMRM; Seattle. 2006. p. 364
16. Glover GH, Pelc NJ. A rapid-gated cine MRI technique. Magn Reson Annu 1988:299–333. [PubMed: 3079300]
17. Hargreaves BA, Vasanawala SS, Nayak KS, Hu BS, Nishimura DG. Fat-suppressed steady-state free precession imaging using phase detection. Magn Reson Med 2003;50:210–213. [PubMed: 12815698]
18. Park J, Larson AC, Zhang Q, Simonetti O, Li D. 4D radial coronary artery imaging within a single breath-hold: cine angiography with phase-sensitive fat suppression (CAPS). Magn Reson Med 2005;54:833–840. [PubMed: 16149060]
19. Griswold MA, Kannengiesser S, Heidemann RM, Wang J, Jakob PM. Field-of-view limitations in parallel imaging. Magn Reson Med 2004;52:1118–1126. [PubMed: 15508164]
20. Derbyshire JA, Herzka DA, McVeigh ER. S5FP: spectrally selective suppression with steady state free precession. Magn Reson Med 2005;54:918–928. [PubMed: 16155880]

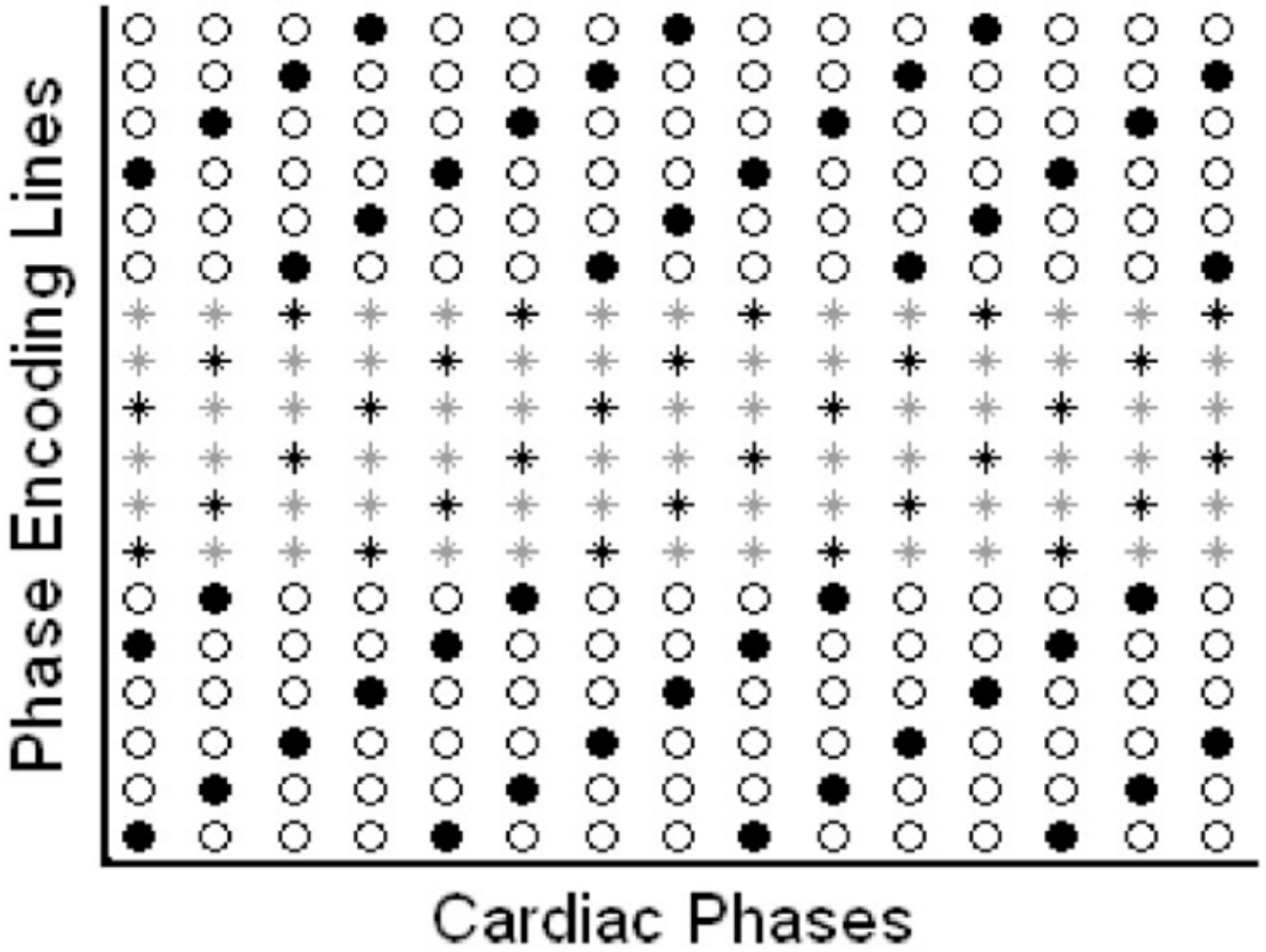

Figure 1.

The sampling pattern of k-t GRAPPA with an acceleration factor in outer *k*-space (AFO) of 4 and k-t^2 GRAPPA with an AFO of 4 and an acceleration factor in center *k*-space (AFC) of 3. The column and the row indicate the phase-encoding direction and the temporal direction, respectively. The black dots represent the acquired outer *k*-space lines, whereas the circles represent the skipped *k*-space lines. Stars represent the ACS lines at center *k*-space. ACS lines were fully acquired for k-t GRAPPA, whereas only the ACS lines represented by black stars were acquired for k-t^2 GRAPPA.

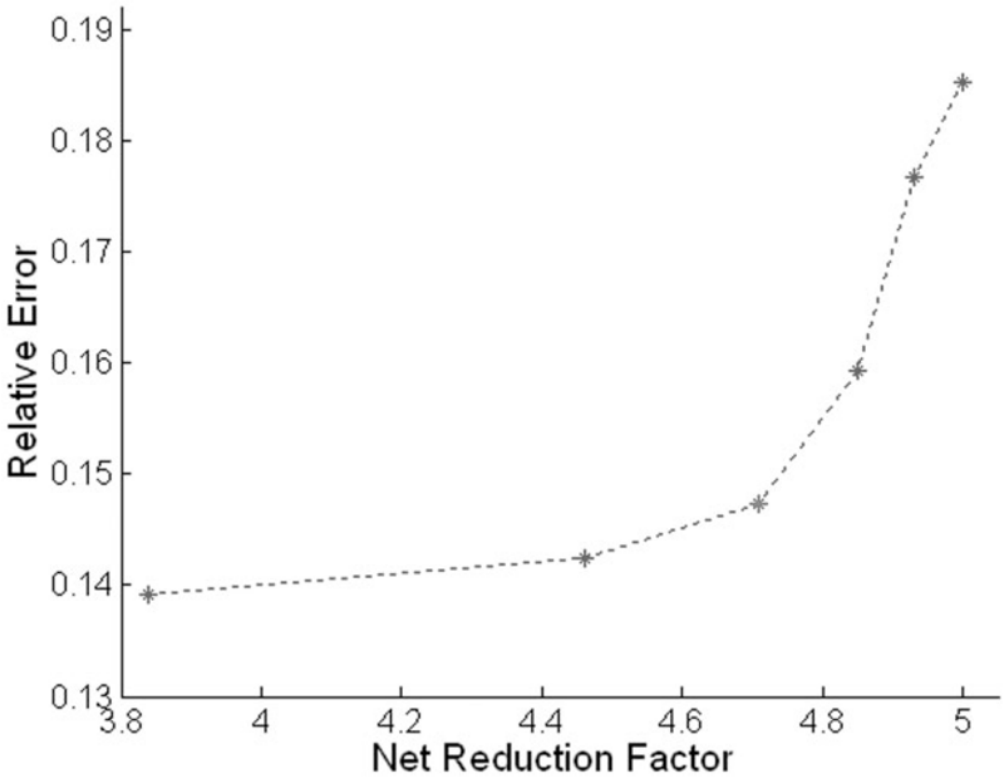

Figure 2.
Mean relative errors for k-t^2 GRAPPA with acceleration factors in center *k*-space (AFCs) of 1~6 (from left to right).

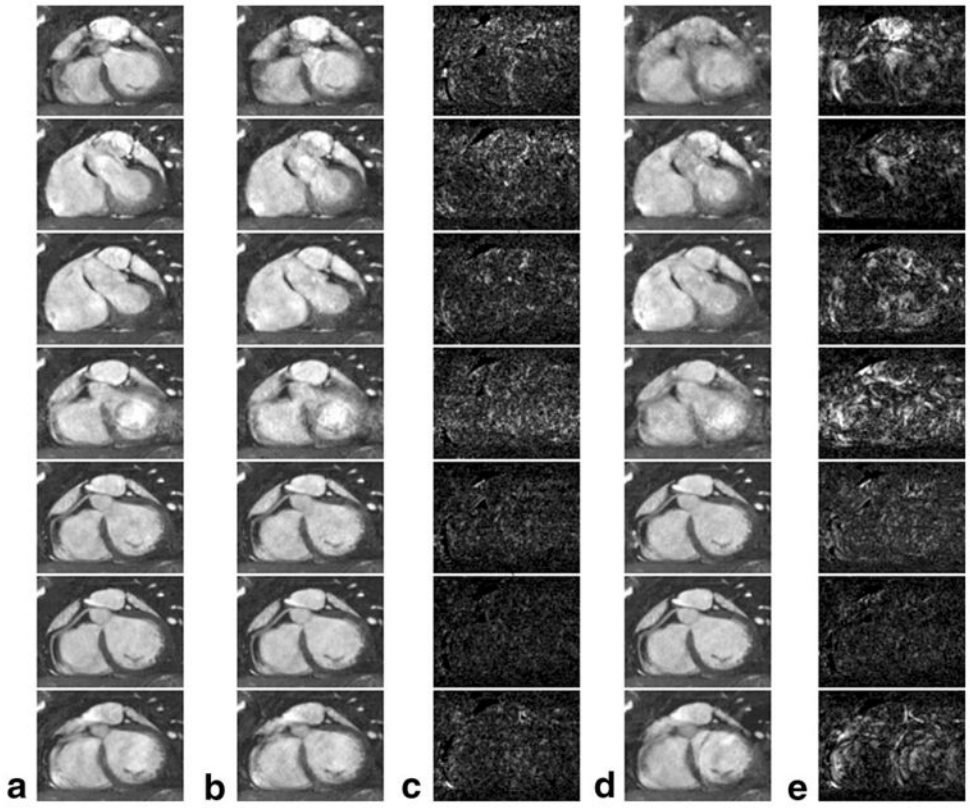

Figure 3.

a: The reference maximum-intensity-projection citation(MIP) images at cardiac phases 2, 4, 6, 8, 10, 12, and 14 (from top to bottom), respectively. **b,c:** The k-t GRAPPA MIP images with an acceleration factor in outer *k*-space (AFO) of 4 and the absolute differences from a at the corresponding cardiac phases, respectively. **d,e:** The corresponding k-t^2 GRAPPA images with an AFO of 4 and an acceleration factor in center *k*-space (AFC) of 3 and the corresponding absolute differences from a, respectively. For clearer demonstration, the gray level in c and e was scaled up by a factor of 5.

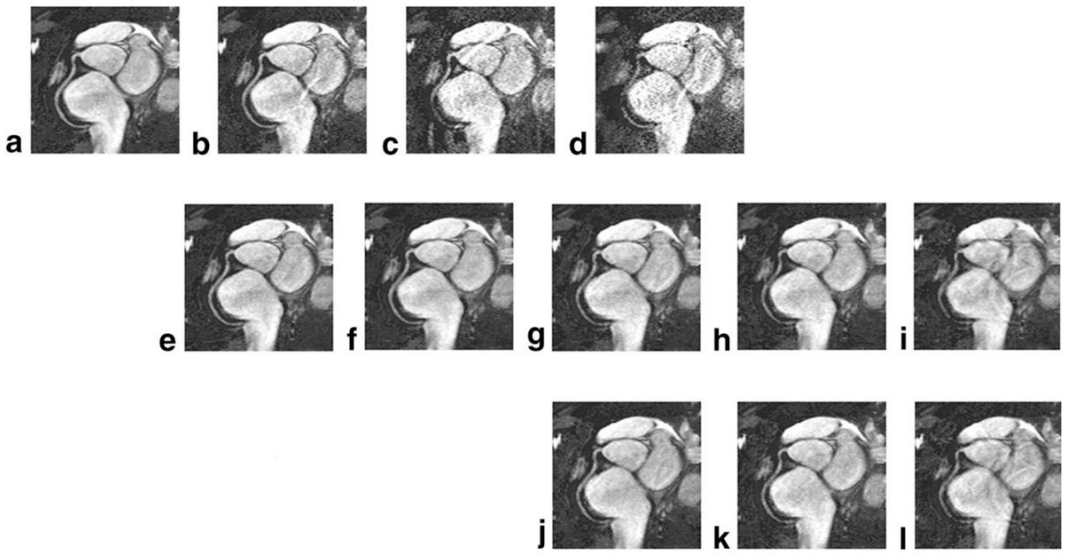

Figure 4.

The maximum-intensity-projection citation(MIP) images reconstructed using different methods: the reference image at mid-diastole (**a**), the corresponding GRAPPA images with acceleration factors in outer *k*-space (AFOs) of 2–4 (**b–d**), the k-t GRAPPA images with AFOs of 2~6 (**e–i**) and the k-t^2 GRAPPA images with AFOs of 4–6 (**j–l**).

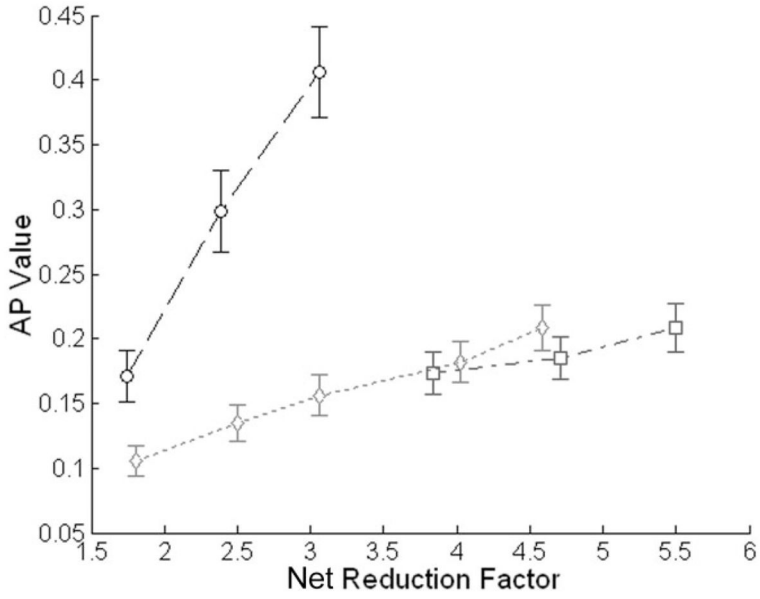

Figure 5.
Mean artifact power (AP) values of the GRAPPA (dashed circles), k-t GRAPPA (dotted diamonds), and k-t^2 GRAPPA (dash–dot squares) images with various acceleration factors in outer *k*-space.

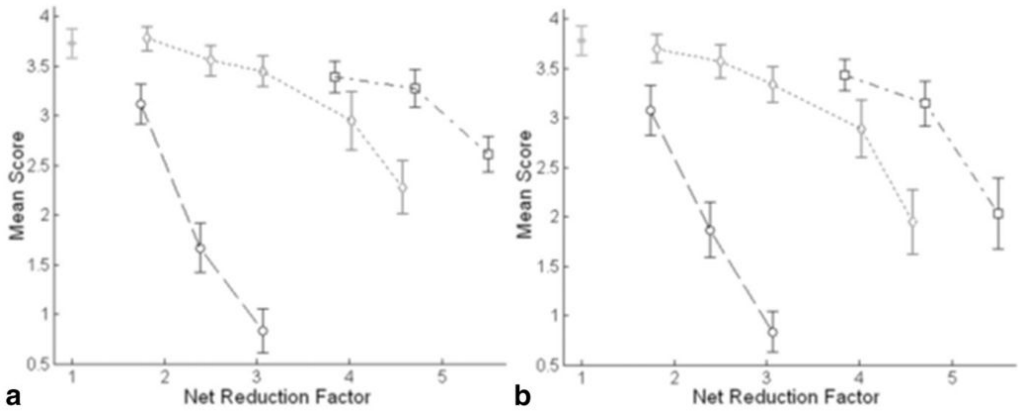

Figure 6.
Mean scores of the reference (solid dot), GRAPPA (dashed circles), k-t GRAPPA (dotted diamonds) and k-t^2 GRAPPA (dash–dot squares) images from reviewer 1 (**a**) and reviewer 2 (**b**).

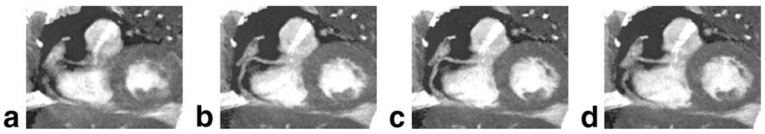

Figure 7.
a–d The diastolic images acquired using true k-t^2 GRAPPA sampling at cardiac phase 13, 15, 17, and 19, respectively.

Table 1

Sampling Parameters of GRAPPA, k-t GRAPPA, and k-t^2 GRAPPA (AFC = 3)*

AFO	**2**		**3**		**4**			**5**		**6**	
Method	GRA	KTG	GRA	KTG	GRA	KTG	KT^{2}G	KTG	KT^{2}G	KTG	KT^{2}G
ACS line number	24	16	20	16	16	16	18	9	15	9	15
Reduction factor	1.74	1.81	2.39	2.50	3.06	3.06	3.84	4.02	4.71	4.58	5.50

*AFC = acceleration factor in center *k*-space; AFO = acceleration factor in outer *k*-space; GRA = GRAPPA; KTG = k-t GRAPPA; KT^{2}G = k-t^2 GRAPPA; ACS = autocalibration signals.